

Férid KOURDA

Hajer ZARDOUM

Regular paper

## Design and Performance Analysis of a Series-Parallel Resonant Converter for Contactless Electrical Energy Transmission

*Abstract - Contactless electrical energy transmission (C.E.E.T) is a manner of electrical energy transmission with no physical contact between the power supply and the load. The resonant converter is one of the most suitable converters for the C.E.E.T. This paper summarises the design procedure of a series-parallel resonant converter used to supply a (24V-50A) battery charger via a contactless transformer having a 1 cm air-gap. A combined frequency and time domain simulation method for studying the resonant converter is presented. The method allows to predict the real behaviour of the converter and to choose the operating frequency, thus permitting to carry out practical non-destructive tests on the real prototype of the battery charger. Experimental results are presented to show the good performances of our analyses.*

**Key words:** contactless transformer, resonant converter, high-frequency, first harmonic method, experimental results.

### I. INTRODUCTION

**C**ontactless Electrical Energy Transmission (C.E.E.T) is a manner of transmitting energy when the use of wires and connectors is not practical, such as for the moving systems, or when it is prohibited as in the case of explosive or wet environments. The C.E.E.T system shown in Fig.1. assures electrical energy transmission from a transmitter (power supply) towards a receiver (load) via a large air-gap transformer. The primary side of the transformer is fed by a high-frequency inverter; the secondary side feeds the load through a rectifier. The use of an air-gap permits a safe electrical energy transfer without any electrical or physical contact between the power supply and the load [1], [2], [7], [8], [9],[10].

This separation involves a large leakage inductance [2]. Moreover a large air-gap leads to a low magnetizing inductance, and consequently more important conduction losses. For these reasons the most suitable converter for this type of transmission is the resonant converter, since its resonant circuit is built only by adding a capacitor to the leakage inductance of the transformer. Moreover it is also a soft-switching converter which allows a frequency increase (to reduce the weight and the volume of the transformer) and thus reduction in commutation losses.

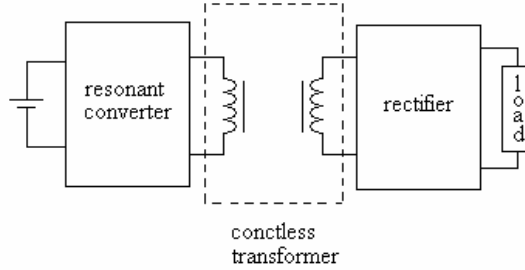


Fig.1 Bloc diagram of the C.E.E.T System

## II. RESONANT CONVERTERS USED IN THE C.E.E.T SYSTEM

The DC-DC resonant converter consists of two conversion stages: a DC-AC intermediate stage consisting of a high-frequency resonant inverter, and an AC-DC H-F stage. In this paper, we are interested in studying the resonant inverter, which can be of two types [3]: a full-bridge resonant inverter, or a half-bridge resonant inverter. The former, composed of four switches and the resonant circuit, is used in high power and for PWM applications. Whereas the latter has only two switches, the two others are replaced by capacitors. These capacitors are used to build the resonant circuit or to make a capacitive medium point. The resonant circuit consists of a combination of inductances and capacitors and the type of the converter is defined according to the number and to the connection of these elements (series, parallel...). We are going to focus on the basic resonant converters, and on their frequency responses.

### A. The Series Resonant Converter

This converter is the most commonly used, because of the simplicity of its realization and study. The resonant circuit is composed of an inductance and a capacitor connected in series as shown in Fig. 2. The simulations of the circuit transfer function ( $V_s/V_e$ ) for various loading levels ( $R_1 < R_2 < R_3 < R_4$ ) and of the input impedance ( $Z_e$ ) phase angle are presented in Fig. 3.

The resonant frequency of the converter is expressed by equation (1).

$$f_0 = \frac{1}{2\pi\sqrt{LC}} \tag{1}$$

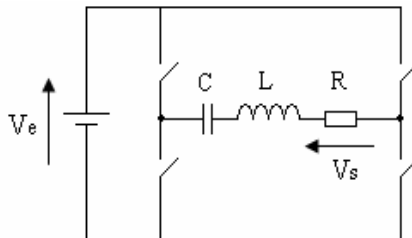


Fig.2 Series resonant inverter

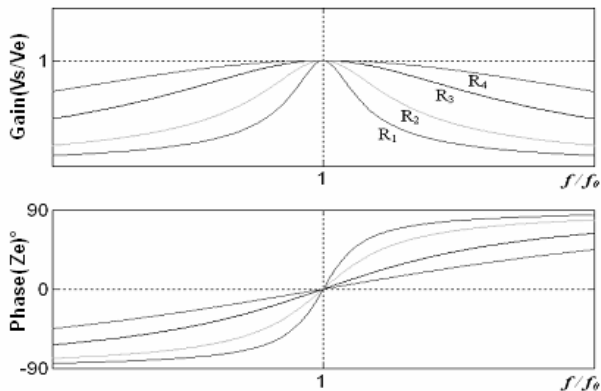


Fig.3 Frequency response of a series resonant converter

We note two operating regions: for frequencies lower than  $f_0$  the angle difference between the voltage and the current is negative, corresponding to a zero-current switching (ZCS) region, for those higher than  $f_0$  the phase difference is positive and corresponds to a zero-voltage switching (ZVS) region. At resonance the current and the voltage are in phase, thus to minimize the reactive power, it is necessary to work very close to this frequency. For a given load, the control of the output voltage may be achieved by action on the frequency: in the ZVS mode a small frequency increase decreases the gain and in the ZCS mode a small frequency decrease makes the gain decrease. However, this control is less effective for light loads because the gain changes quickly with frequency.

**B. The parallel Resonant Converter**

The parallel resonant converter (shown in Fig.4), based on a current inverter, is the dual of the series resonant inverter. The operation of this inverter is similar to the series inverter with simply replacing the voltage source by a current source.

**C. Multi-element Resonant Converter**

Resonant converters with more than two elements have good control characteristics [3], but they contain the more components, penalizing in terms of losses, density and cost, which makes structures with more than three elements scarce [4].

Fig.5 represents an example of a resonant converter (CL3) with four resonant elements [4]. This converter has the advantage that the various gain curves pass by a particular point located at a frequency equal to 1.15 times the resonant frequency. If the converter is designed to operate at or near this point, it would be possible to control the output voltage by slightly varying the frequency [4].

In this work, the authors study a 5 elements resonant converter used as a power circuit for a contactless battery charger. The resonant circuit is composed of three inductances and two capacitors, where the inductances are those of the contactless transformer model shown in Fig. 6.

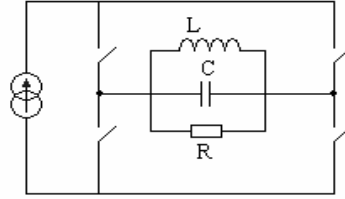


Fig.4 Parallel resonant inverter

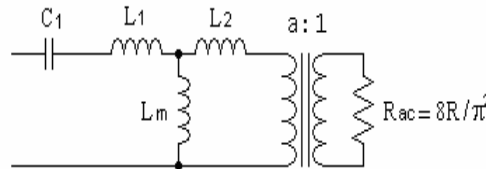


Fig.5 Equivalent circuit of a series-parallel resonant converter [4]

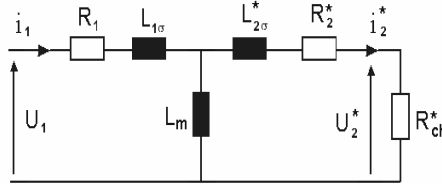


Fig.6 Equivalent model of the transformer used in the C.E.E.T

### III. STUDY AND SIMULATION OF THE POWER CIRCUIT OF THE CONTACTLESS BATTERY CHARGER

The circuit diagram of the proposed converter is shown in Fig. 7. It comprises a half-bridge capacitive inverter fed by a DC voltage  $E$ , and composed of two switches with two anti-parallel diodes and two resonant capacitors  $C_{1H}$  and  $C_{1L}$ .

The inverter feeds the contactless transformer, the secondary of the transformer, which is an inductive half-bridge; feeds a rectifier through a third resonant capacitor  $C_2$ . The filtering stage comprises, a smoothing inductance  $L_f$ , a filtering capacitor  $C_f$  and is loaded by a resistance  $R_{ch}$ . Note that the converter shown in Fig. 7 is equivalent to the circuit diagram of fig. 8 by letting  $C_1=C_{1H}+C_{1L}$ . We choose to command the switches via two complementary control signals having a duty cycle equal to 0.5. When the switch  $K_H$  leads, the voltage  $U_{AB}$  across the dipole AB is equal to  $E$ , and when  $K_L$  leads it is zero, thus we can replace the dipole AB by a square signal generator of a magnitude equal to  $E$  and operating at the switching frequency.

Replacing the transformer by its equivalent model [5] and the dipole AB by its equivalent generator, we get the power circuit of Fig. 9, where  $L_1$  is the primary leakage inductance,  $L_2$  is the secondary leakage inductance and  $L_m$  is the magnetizing inductance of the transformer.

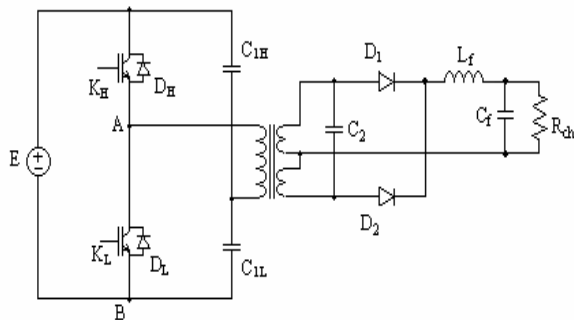


Fig.7 Circuit diagram of the converter

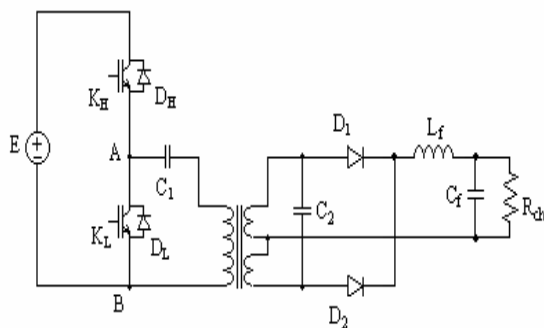


Fig.8 Equivalent circuit diagram of the converter

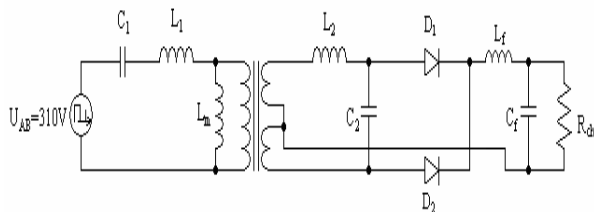


Fig.9 Resonant circuit fed with a square voltage generator

**A. Calculation of the resonant circuit transfer function by the first harmonic method**

According to an undertaken research in [6] on the error generated by the first harmonic method in a resonant converter study, it was shown that when the switching and the resonant frequencies are equal, the error is zero, and the farther we move from it the more the error becomes important. This is explained by the fact that at resonance the current is sinusoidal and is equal to its first harmonic. Moving away from resonance, the current is no more sinusoidal and contains more harmonics, resulting in a difference between the signal and its first harmonic component.

**1) Application of the first harmonic method on the primary side:**

In order to study analytically the frequency response of the converter, the first harmonic method is used. The square voltage generator ( $U_{AB}$ ) is replaced by a sinusoidal generator corresponding to the first component of the harmonic decomposition of its equivalent alternative square wave: the voltage  $U_{AB}$  is fragmented into a continuous dc component  $U_{AB(=)}$  and an alternating component  $U_{AB(ac)}$  as shown in Fig. 10. The dc component remains

constant at the capacitor  $C_1$  and does not affect the energy transfer, only the alternating component intervenes.

The voltage  $U_{AB}$  is given by:

$$U_{AB} = U_{AB(=)} + U_{AB(ac)} \quad (2)$$

The decomposition in Fourier series of the voltage  $U_{AB(ac)}$  is expressed as follows:

$$U_{AB(ac)}(t) = \frac{4U_{AB(ac)}}{\pi} \sum_{n=1,3,5,\dots} \frac{1}{n} \sin(2\pi nft) \quad (3)$$

Let  $U_{AB(ac)1}$  be the first harmonic component of the signal  $U_{AB(ac)}$ , named  $V_e(t)$ . The magnitude of  $V_e(t)$  is:

$$\frac{4U_{AB(ac)}}{\pi} = 1.27 \cdot U_{AB(ac)} = 1.27 \cdot \frac{E}{2}$$

$$V_e(t) = 0.9 \frac{E}{2} \sqrt{2} \sin(2\pi ft) \quad (4)$$

The square signal is then approximated by a sinusoidal generator having an rms value of  $0.9 E/2$  and operating at the switching frequency.

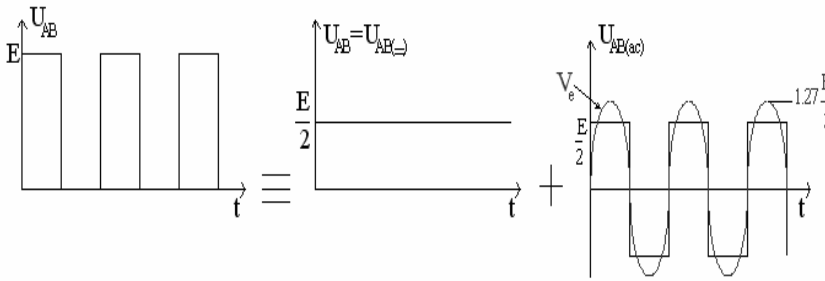


Fig.10 Decomposition of the voltage  $U_{AB}$

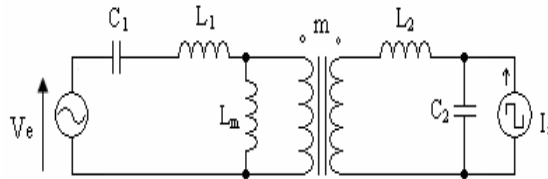


Fig.11 The equivalent circuit of the converter with the load replaced by its square equivalent current generator

**2) Application of the first harmonic method on the secondary side:**

We assume that the values of the smoothing inductance  $L_f$  and the filtering capacitor  $C_f$  are high enough so that the current and the voltage across the load are held constant.

Let  $I_s$  be the current in the inductance  $L_f$ . When the diode  $D_1$  is on the current resulting from the medium point of the transformer is equal to  $I_s$  and when the diode  $D_2$  is on it is equal to  $-I_s$ .

Replacing in Fig.9 the voltage  $U_{AB}$  by its first harmonic equivalent generator and the load by the square current generator, we obtain the equivalent circuit shown in Fig.11.

Let  $I_{s1}$  be the sinusoidal current generator, that is equivalent to the first harmonic of the square generator  $I_s$ , its rms value is:

$$I_{s1rms} = \frac{4}{\sqrt{2 \cdot \pi}} \cdot I_{srms} = 0.9 I_{srms} \tag{5}$$

And  $R_{ch1}$  be the equivalent load resistance determined to maintain the same output power of the initial circuit and of the first harmonic method equivalent circuit (Fig 12).

$$P_s = R_{ch1} \cdot I_{s1rms}^2 = R_{ch} \cdot I_{srms}^2 \tag{6}$$

$$R_{ch1} = R_{ch} \cdot \frac{I_{srms}^2}{I_{s1rms}^2} \tag{7}$$

Replacing in (7)  $I_{s1rms}$  by its expression given by (5)  $R_{ch1}$  is given by:

$$R_{ch1} = \frac{\pi^2}{8} \cdot R_{ch} = 1.234 R_{ch} \tag{8}$$

Two resonant frequencies could be identified for the resonant circuit of Fig. 13.

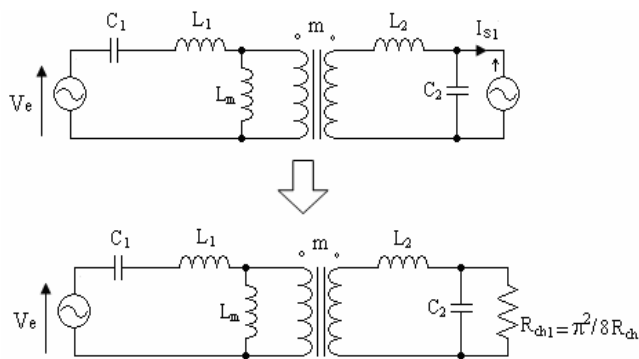


Fig.12 Circuit diagram of the converter obtained by the first harmonic method

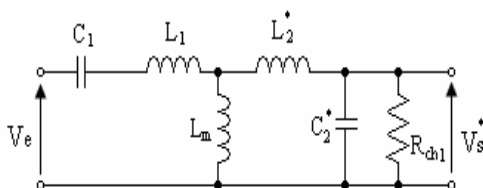


Fig.13 Equivalent resonant circuit brought back to the primary side

The resonant frequency obtained with the transformer secondary short-circuited is:

$$f_1 = \frac{1}{2 \cdot \pi \cdot \sqrt{C_1 \cdot \left( L_1 + \frac{L_m \cdot L_2^*}{L_m + L_2^*} \right)}} \tag{9}$$

The resonant frequency seen from the secondary side when the primary is open is:

$$f_2 = \frac{1}{2 \cdot \pi \cdot \sqrt{C_2^* \cdot (L_m + L_2^*)}} \quad (10)$$

Giving:

$$\gamma_2 = \frac{L_2^*}{L_m}, \quad \beta = \frac{C_2^*}{C_1}, \quad a = \frac{1}{m}$$

The transfer function of the resonant circuit  $T = \frac{V_s}{V_e}$  is given by expression (11).

The simulation parameters are given in table I. They were determined by a finite elements simulation method [5]. The number of the transformer primary turns is  $N_1 = 12$  while the secondary winding has only one wire,  $N_2 = 1$ .

$$T = \frac{1}{a \left[ \left( 1 + \gamma_1 - \frac{1}{L_m C_1 \omega^2} \right) \left( 1 - L_2^* C_2^* \omega^2 \right) + \beta - L_1 C_2^* \omega^2 \right] + j \left[ \frac{(L_m^2 (\gamma_1 + \gamma_2 (1 + \gamma_1))) \omega}{a R_{eH} L_m} - \frac{L_m (1 + \gamma_2)}{a R_{eH} L_m C_1 \omega} \right]} \quad (11)$$

TABLE. I : Simulation parameters

$L_1$	$L_2^*$	$L_m$	$C_1$	$C_2$
4.54 $\mu$ H	6.31 $\mu$ H	8.47 $\mu$ H	140nF	11 $\mu$ F

Simulations of the transfer function and of the different waveforms of the dimensioning parameters (the input impedance, the resonant capacitor voltage, the input current...) of the converter are shown in Fig.14.

Simulations results show that there are three particular frequencies: low  $f_L = 103$ kHz, medium  $f_m = 150$ kHz and high  $f_H = 217$  kHz, these frequencies are characterized by a zero angle difference between the input current and the input voltage of the circuit.

The frequency  $f_m$  seems to be a good operating frequency, indeed the input impedance is at its maximum. Consequently, the voltage across the resonant capacitor  $C_1$ ,  $V_{c1max}$  is lower than 150V and the primary current  $I_{inmax}$  is lower than 20A for the different loads, allowing an easy dimensioning of the resonant capacitors and of the switches. The curves show the existence of a very interesting range of frequencies where the voltage is steady whatever the load is. This range is situated in the middle of the interval centred on  $f_m$  and located between  $f_L$  and  $f_H$ , so it facilitates the voltage control when the frequency varies around  $f_m$ . It should be noted that the frequencies  $f_L$  and  $f_H$  might be destructive since the input

impedance is very low which may generate an important current in the inverter and a very high voltage across the resonant capacitor  $C_1$

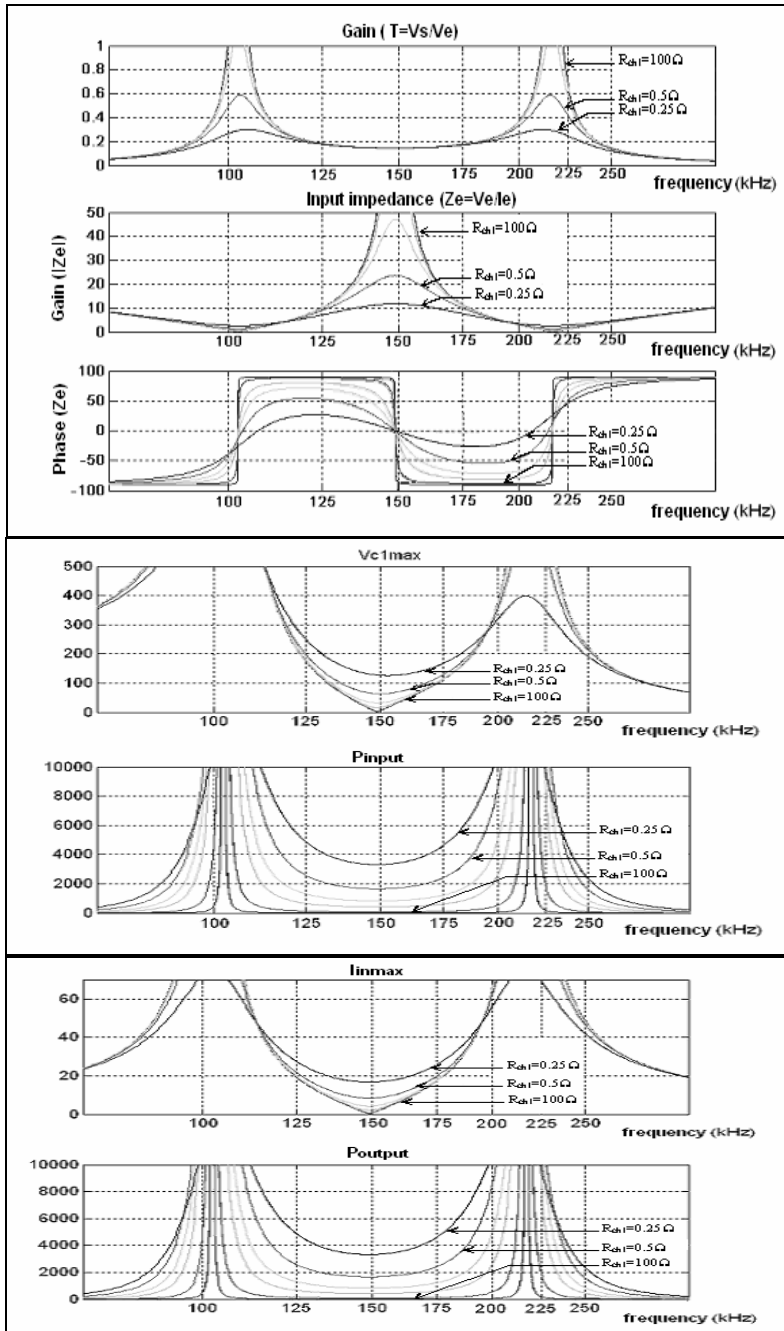


Fig.14 Simulation of the transfer function and the various dimensioning parameters of the converter versus frequency

**B. Time domain response simulation of the resonant circuit**

So far, the resonant circuit (nonlinear system) was transformed with the first harmonic method ; then its transfer function was calculated, and its various resonant frequencies were identified from its frequency response.

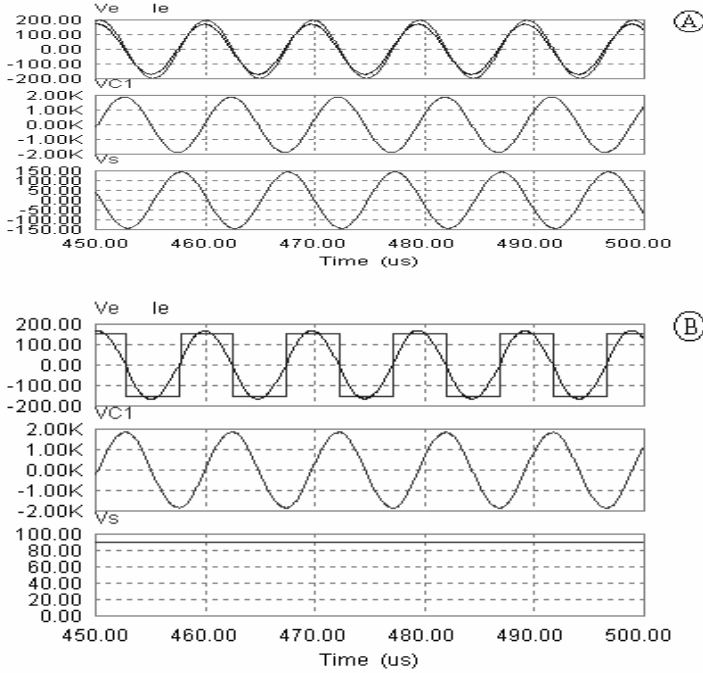


Fig.15 Input current, input voltage and output voltage simulations at  $f_L = 102.7$  kHz

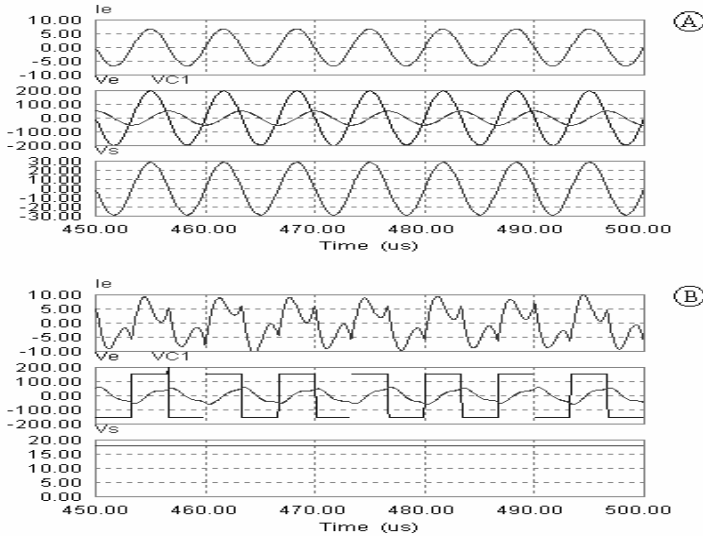


Fig.16 Input current, input voltage and output voltage simulations at  $f_m = 150$ kHz

Next to, verify the effectiveness of the frequency analysis of the converter, time domain simulation will be performed at the different resonant frequencies. (Fig.15) and (Fig.16) show a comparison of the obtained time domain simulation. In A are shown the simulations of the first harmonic method equivalent circuit (Fig.12), and in B are shown the simulations of the initial circuit (Fig.9).

It can be seen from these stimulations that the first harmonic method results are verified for the frequencies  $f_L$  and  $f_H$ , in fact the primary current and voltage are in phase. Moreover, at the frequency  $f_m$  we obtain the same output voltage for the two circuits.

On the other hand, the primary current, contrarily to what expected, is not sinusoidal at this frequency, for the influence of the higher order harmonics seems to be not negligible.

In Fig.18 are presented the simulation result of the primary current waveform for various loads at the operating frequency  $f_m$ . It is shown that the weaker the load is, the closer the primary current shape is to sinusoidal. To better illustrate the influence of the load on the primary current waveform, the harmonic currents and the harmonic rate of distortion for each load are calculated and are shown respectively in Fig. 19 and Fig. 20.

The results show that while harmonics 3, 5 and 7 are constant for any load value, the first harmonic decreases exponentially and dominate for small loads. This explains the sinusoidal current shape for small load values (Fig.18 d).

We can also see that for small loads, the harmonic distortion rate is very small. The more the load increases the more it tends towards 1, and consequently the error of the first harmonic method is about 100%.

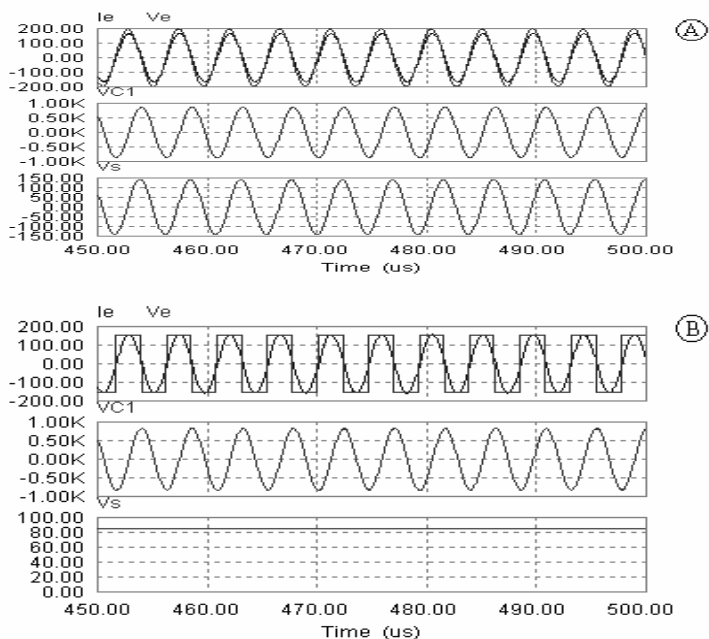


Fig.17 Input current, input voltage and output voltage simulations at  $f_H = 217$  kHz

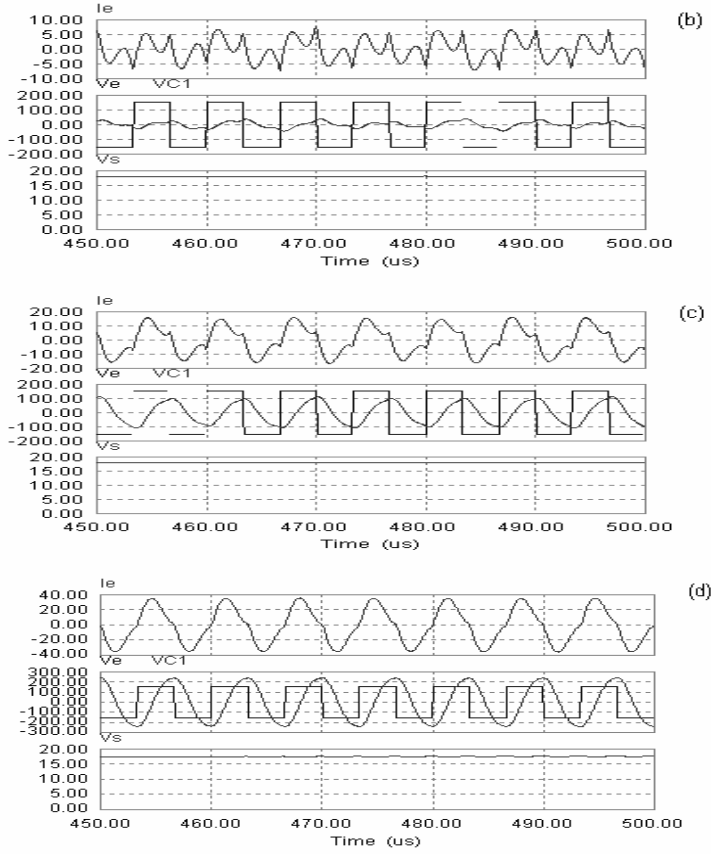


Fig.18 Simulation at  $f_m=150$  kHz ( $R_{ch}=10 \Omega$  (a);  $1\Omega$  (b) ;  $0.25\Omega$  (c) ;  $0.1\Omega$  (d))

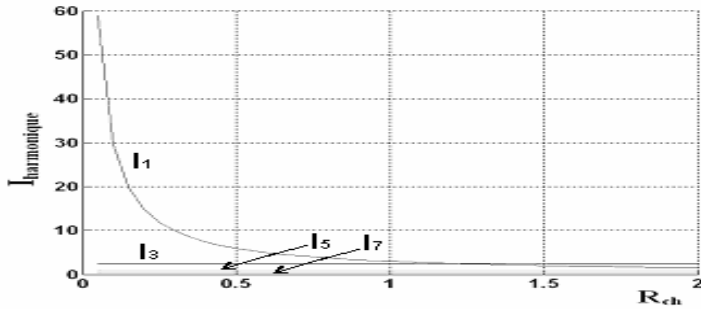


Fig.19 Harmonic currents  $I_1, I_3, I_5$  and  $I_7$  versus the load

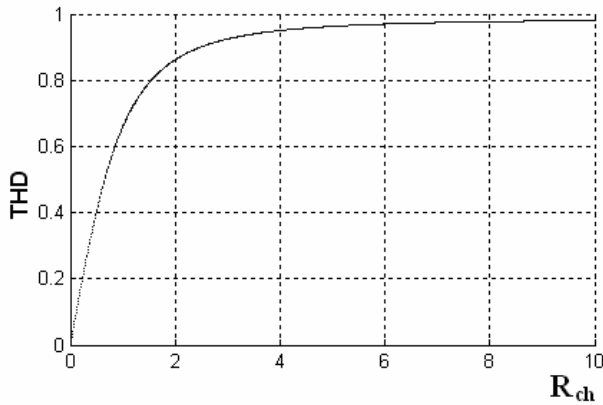


Fig.20 Harmonic rate of distortion versus the load at  $f = f_m = 150$  kHz

#### IV. EXPERIMENTAL RESULTS

##### A. Low input voltage Tests

We made our C.E.E.T circuit of the battery charger with a planar transformer having a 1cm air-gap. The transformer was built using Philips 64/10/50 ferrite cores (photo in Fig.23). The transformer primary winding of 12 turns is made on a printed circuit board, it is a multi-layer multi- turn winding, and the secondary has only one planar turn made of aluminium. We partitioned the primary winding into two double faces PCB, each one comprises three turns. The offset films of the two faces are shown in Fig. 22, Fig. 21 represents the cross-section of the transformer; the turns are numbered according to the direction of the winding.

According to the simulation results carried out in the last sections, the resonant capacitor voltage and the primary current are very high at the frequencies  $f_L$  and  $f_H$ . In order to avoid the converter destruction during the experimental tests a frequency sweeping was made with a reduced supply voltage,  $E=30V$ . Once the frequency response of the circuit and the various resonant frequencies were identified, we could increase the supply voltage while maintaining a non-destructive operating frequency, which should be very close to  $f_m$ .

Fig. 24~Fig.32 show the different experimental tests and plots performed in order to identify the resonant frequencies of the circuit, which were worth :  $f_L=146$  kHz,  $f_m=196$  kHz and  $f_H=249$  kHz.

Fig. 24~ Fig.26 show the measurements taken around the frequency  $f_L$  :

At the frequency  $f=141kHz < f_L=146kHz$  the commutation is of type ZCS, exhibiting a negative voltage drop on  $V_{KL}$  due to the conduction of the diode  $D_L$ .

At the frequency  $f=146kHz$  which is very close to the resonant frequency  $f_L$ , the primary current  $I_e$  is almost sinusoidal as shown in Fig.25.

The experimental and the simulations results are in agreement : it is checked that for  $f < f_L$  the commutation is ZCS; at  $f=f_L$  the primary current and voltage are in phase (fig.25 right), at  $f > f_L$  the commutation is ZVS. We point out that the frequency  $f_L$  is dangerous because the capacitor  $C_{1L}$  voltage value is  $V_{C_{1L,max}} = 94V$  for a supply voltage  $E=30V$ , so it would be  $V_{C_{1L,max}} = 940V$  for a nominal voltage  $E_N=300V$ . Likewise, the primary current which value

$I_{rms}=2A$  for  $E=30V$ , would reach 20A for the nominal voltage. Moving away from this frequency during high voltage tests is thus necessary.

Fig.27~Fig.29 show the measurement results taken around  $f_m$ . At  $f=180kHz < f_m=196kHz$  the commutation is ZVS as shown in Fig. 27. At  $f=196kHz$  we are very close to the resonant frequency  $f_m$  but slightly in the ZVS mode as it can be noticed from the current waveform of Fig.28. We can also see that when the voltage  $V_{CIL}$  is of value  $V_{CILmax}=32V$ , the current  $I_{rms}=0.23A$ , these values would be multiplied by ten for the nominal supply voltage  $E_N=300V$  and are still small. This is advantageous for an easy and safe dimensioning of the capacitors  $C_{1L}$ ,  $C_{1H}$  and of the switches  $K_L$  and  $K_H$ .

Near the resonant frequency  $f_m$  important oscillations with a high  $dv/dt$  appear as seen in Fig. 28, this may be interpreted as follows :

When the switch  $K_H$  is turned off, a slightly reactive current is established through the diode  $D_L$  which leads during the time  $t_1$ , but during this conduction time,  $K_L$  would have been started, which is not really the case. During the time  $t_2$  all switches are off, point A in Fig.7 is floating and theoretically its voltage must oscillate to stabilize at the level  $E/2$ . When  $t_2$  is over, the switch  $K_L$  is turned on after a dead time  $t_m=t_1+t_2=200ns$ . These oscillations of the voltage  $V_{KL}$  generate important  $dv/dt$  which induces capacitive currents  $i=C.dv/dt$  through the parasitic capacitors of the drain-gate junction of the switch and disturb the control signal. This phenomenon is strongly amplified when the supply voltage  $E$  is increased.

One solution to that problem consists of ensuring a reactive current, which would increase the diode  $D_L$  conduction time.

At the frequency  $f=213 kHz > f_m =196 kHz$  in Fig. 29 the commutation is ZCS. The arrows seen on the voltage  $V_{KL}$  show the conduction of the diode  $D_L$  at the end of the half-period, this time of conduction indicates the presence of a small reactive current. The arrows with the cross in Fig.29 point to the turning off times of the switch. The beginning of the diode short conduction due to the absence of reactive current is reflected on the voltage waveform of the switch.

The experimental results around  $f_m$  are compatible with those of the simulation. Indeed at  $f < f_m$  the commutation is ZVS, at  $f = f_m$  the primary current and the voltage are in phase, and at  $f > f_m$  the commutation is ZCS.

The frequency  $f_m$  is a good operating frequency, since it offers the opportunity to work either at lower or higher frequencies without the need of any switch oversizing.

Fig. 30~ Fig.32 show measurements taken around  $f_H$ , at  $f=224 kHz$  we have the ZCS mode with a small reactive current. The capacitor  $C_{1L}$  voltage is worth  $V_{CILmax}=30V$  and the primary current is worth  $I_{crms}=0.85A$ .

At  $f = f_H =249 kHz$  (Fig.31) the primary current  $I_e$  and the voltage  $V_{KL}$  are in phase. However, the voltage across the capacitor  $C_{1L}$  is relatively high,  $V_{CILmax}= 40V$  for a supply voltage  $E=30V$ . For the nominal supply voltage  $E_N=300V$ ,  $V_{CIL}$  would be  $V_{CILmax}= 400V$ . The primary current is also high,  $I_{rms}=1.4A$  for  $E=30V$ , it would be of 14A for the nominal supply voltage. So it is necessary to operate far from this frequency during the high-voltage tests.

At this frequency we see the same phenomenon of  $dv/dt$  as seen at the frequency  $f_m$  due to the absence of reactive current and the high dead time. The experimental results around  $f_H$  confirm those of simulation, we check that for  $f < f_H$  the commutation is ZCS, at  $f = f_H$  the primary current and voltage are in phase, and at  $f > f_H$  the commutation is ZVS.

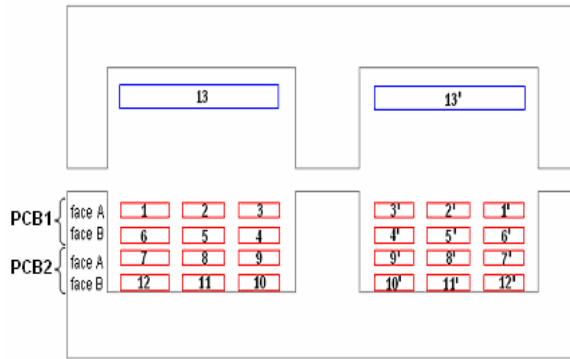


Fig.21 Radial Cross-section of the planar transformer

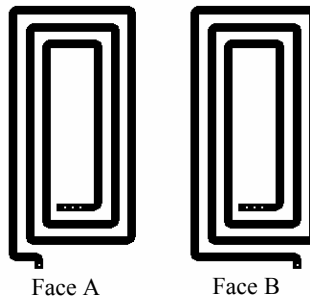


Fig.22 Offset films of the transformer primary winding

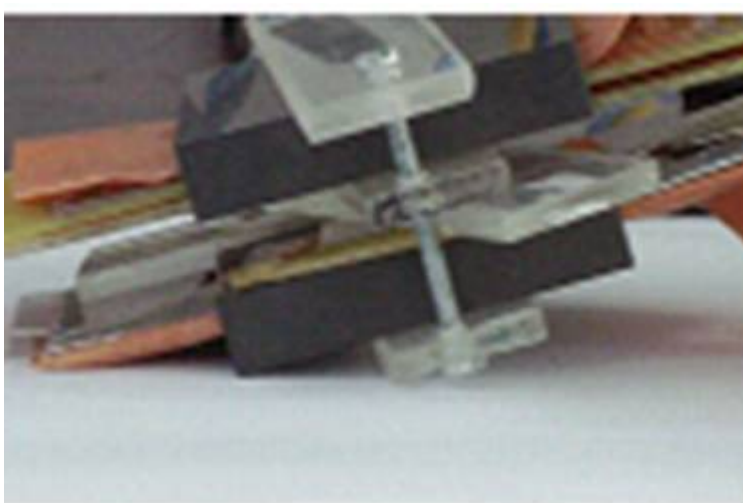


Fig.23 Photo of the planar transformer (air-gap = 1cm)

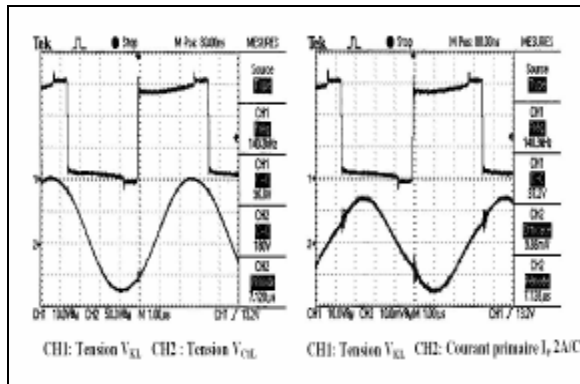


Fig.24 Circuit response at  $f=141 \text{ kHz} < f_L=146 \text{ kHz}$

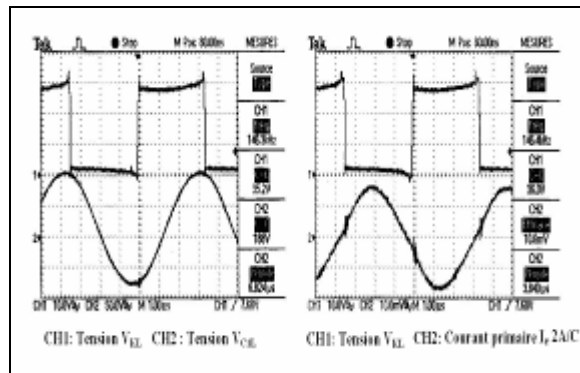


Fig.25 Circuit response at  $f=f_L=146 \text{ kHz}$

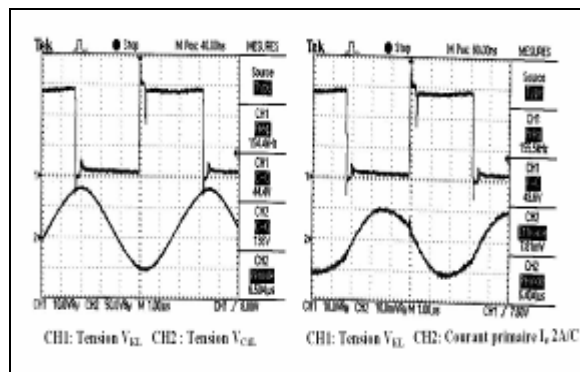


Fig.26 Circuit response at  $f=155 \text{ kHz} > f_L=146 \text{ kHz}$

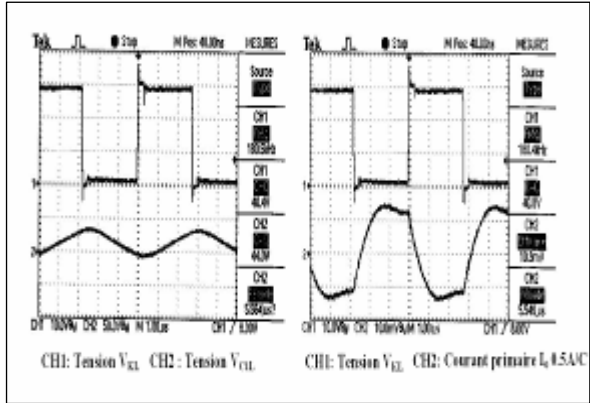


Fig.27 Circuit response at  $f=180 \text{ kHz} < f_m=196 \text{ kHz}$

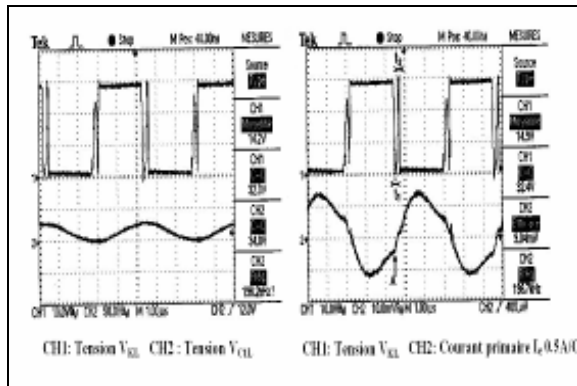


Fig.28 Circuit response at  $f=f_m=196 \text{ kHz}$

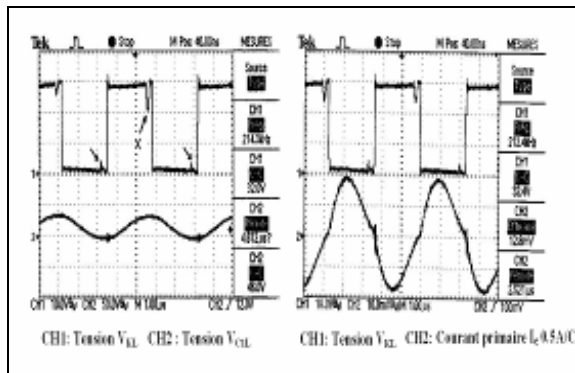


Fig.29 Circuit response at  $f=213 \text{ kHz} > f_m=196 \text{ kHz}$

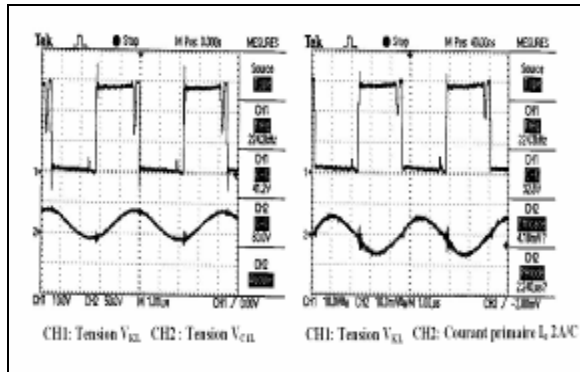


Fig.30 Circuit response at  $f=224 \text{ kHz} < f_H=249 \text{ kHz}$

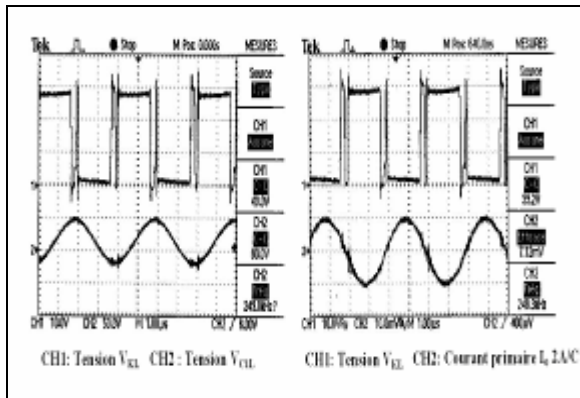


Fig.31 Circuit response at  $f=f_H=249 \text{ kHz}$

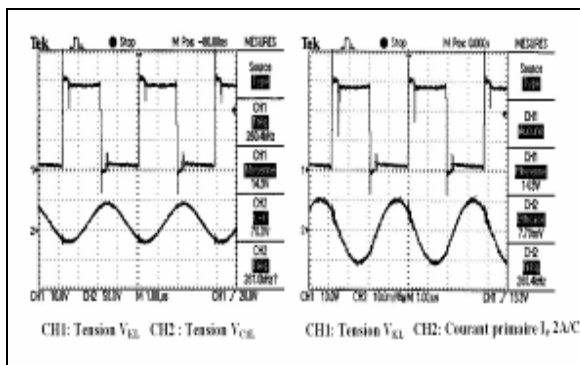


Fig.32 Circuit response for  $f=260 \text{ kHz} > f_H=249 \text{ kHz}$

**B. High input voltage tests**

After having identified the frequency behaviour of the resonant converter, we choose the IRFP360 MOSFET for the switches  $K_H$  and  $K_L$ , each one of them has a snubber capacitor  $C=3.3\text{nF}$  which contributes to reduce the  $dv/dt$ .

We choose to operate in the ZVS mode at a frequency slightly lower than  $f_m=196$  kHz, namely  $f=190$  kHz.

The converter is supplied by a 220V ac rectified and filtered voltage. Experimental waveforms are shown in Fig. 33~ Fig. 34. The voltage  $V_{C_{IL}}$  is worth  $V_{C_{ILmax}}=356$ V, the primary current is almost sinusoidal with a small reactive current, and the maximum is 8A, the average output current is worth  $I_{savg}=25$ A with a ripple  $\Delta I_s=3$ A. The arrows in Fig. 34 indicate the turning off time of the switches showing that we are in the ZVS mode.

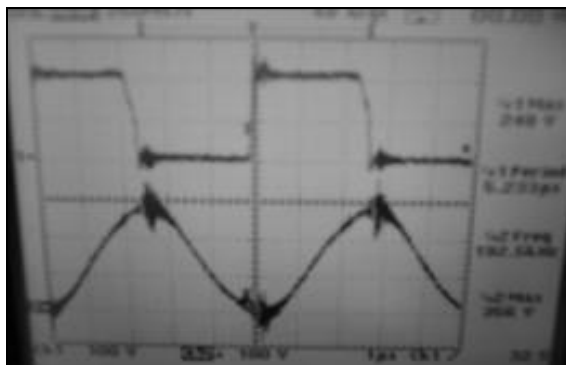


Fig.33 Voltages across the switch  $K_L$  and the capacitor  $C_{IL}$   
 CH1 : Voltage  $V_{KL}=248$ V                      CH2 : Voltage  $V_{CIL}=356$ V  
 CH1period = 5.233 $\mu$ s                      CH2freq=192.5 kHz

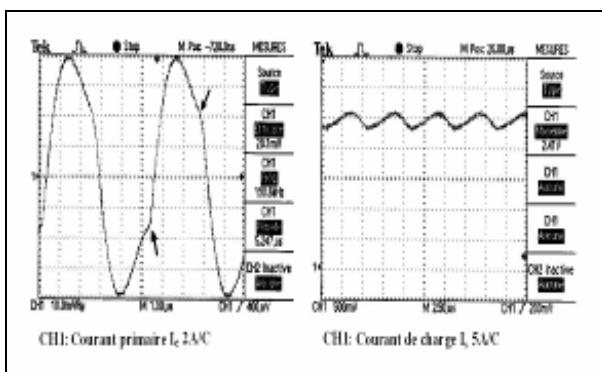


Fig.34 Primary current and load current:  $I_p, I_s$

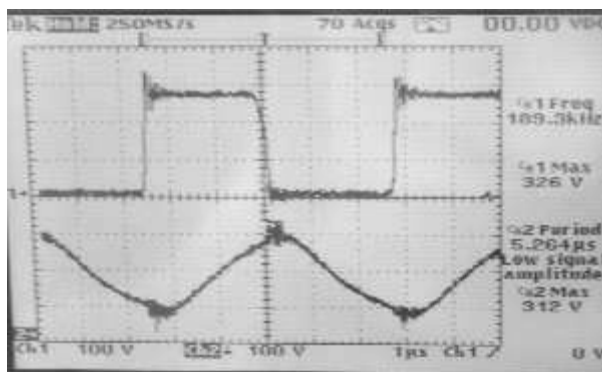


Fig.35 Voltages across the switch  $K_L$  and the capacitor  $C_{1L}$ ,  
 CH1: Voltage  $V_{KL}=326V$ , CH2: Voltage  $V_{C1L}=312V$

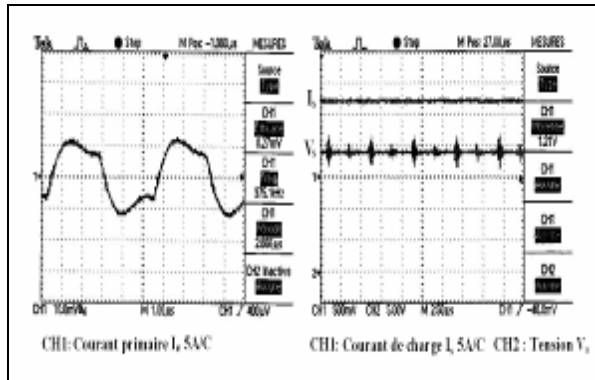


Fig.36 Primary current  $I_e$ , load current  $I_s$  and load voltage  $V_s$ .

## V. CONCLUSION

In this paper a combined frequency and time domain based analysis has been performed to study a 5 elements series-parallel resonant converter used in the C.E.E.T. Being nonlinear the power circuit of the converter is transformed by the first harmonic method to enable an analytical transfer function calculation.

The transfer function simulation of the resonant circuit show the appearance of three resonant frequencies which are characterized, by definition, by a null phase difference between the input current and the input voltage. Time domain simulation around these resonant frequencies was performed, and the operating frequency selection was based on the technological constraints of the switches and the various circuit components.

It was predicted by the frequency response and confirmed by the time simulations that the lower resonant frequency called  $f_L$  and the higher one called  $f_H$  are dangerous. This is because the input impedance of the resonant circuit is very low so the primary current and the resonant capacitor voltage are very high. Moreover it was found that the resonant frequency  $f_m$ , located in the mid-interval  $[f_L, f_H]$  is a good frequency for operation, the input impedance of the resonant circuit is rather high leading to an acceptable primary current and resonant capacitor voltage, allowing an easy and economic dimensioning of the different switches and the resonant capacitors.

The combined frequency and time domain based method of simulation showed that working with such a converter has the following advantage, if operating around the resonant frequency  $f_m$  the gain remains constant, and depending on the type of the commutation (ZVS, ZCS), one has to choose either operating just above or just below the resonant frequency  $f_m$ . If operating above the resonant frequency  $f_m$  the phase difference between the input current and voltage would be negative, the commutation would be of type ZCS and the appropriate switch would be an IGBT with an anti-parallel diode. If one chooses to work under  $f_m$  the input current and voltage angle difference would be positive, the commutation would be of type ZVS and the switch which allows an affordable and easy operation in the ZVS mode at high-frequencies would be a MOSFET.

During the experimental tests done on the resonant converter; we applied a frequency sweeping with a low supply voltage in order to identify the various resonant frequencies of the circuit which coincide with the theoretical prediction, then we have chosen the good

operating frequency  $f_m$  in order to carry out the high voltage tests. The various measurements taken on our converter enabled us to validate the simulation results.

## REFERENCES

- [1] Y. Jang, and M. M. Jovanovic, A contactless electrical energy transmission system for portable-telephone battery chargers, *IEEE Trans. Ind. Electron.*, vol. 50, pp. 520-527, Jun. 2003.
- [2] R. Mecke, Contactless inductive energy transmission systems with large air gap, 9<sup>th</sup> European Conference on Power Electronics and Applications, Graz 2001, Proceedings on CD-ROM.
- [3] I. Batarseh, Resonant converter topologies with three and four energy storage elements, *IEEE Trans. Power. Electron.*, vol. 9, pp. 64-73, Jan. 1994.
- [4] C. Chakraborty, M. Ishida, and Y. Hori, Novel half-bridge resonant converter topology realized by adjusting transformer parameters, *IEEE Trans. Ind. Electron.*, vol. 49, pp. 197-205, Feb. 2002.
- [5] H. Zardoum, F. Kourda, Détermination des Paramètres du Modèle Electrique d'un Transformateur Planar Haute-fréquence, 4<sup>ème</sup> Conférence Internationale, JTEA Hammamet 2006, Proceedings on CD-ROM.
- [6] B. Yang, Topology Investigation for Front End DC/DC Power Conversion for Distributed Power system, Ph. D dissertation, Virginia Polytechnic Institute, Sept. 2003, Blacksburg, Virginia.
- [7] S.Y.R. Hui, Wing W. C. Ho, A new generation of contactless battery charging platform for portable consumer electronic equipment, *IEEE power electronics*, vol.20 n°3 May 2005, pp 620-627.
- [8] R. Mecke, C. Rathge, A. Ecklebe, A. Lindemann, Bidirectional switches for matrix converter in contactless energy transmission systems, European Conference on Power Electronics and Applications, Dresden 2005, Proceedings on CD-ROM.
- [9] J. Lastowiecki and P. Staszewski, Sliding Transformer With Long Magnetic Circuit For Contactless Electrical Energy Delivery To Mobile Receivers, *IEEE Trans. on Industrial Electronics*, vol. 53, No 6, 2006, pp. 1943-1948.
- [10] C.L.W. Sonntag, E.A. Lomonova, J.L. Duarte, A.J.A.Vandenput, Specialed Receivers for Three-Phase Contactless Energy Transfer desktop Applications, pp1-11, EPE 2007.